

An entrainment-based model for annular wakes, with applications to airborne wind energy

Sam Kaufman-Martin¹, Nicholas Naclerio, Pedro May, and Paolo Luzzatto-Fegiz

Department of Mechanical Engineering, University of California, Santa Barbara, 93106, USA

Abstract

Several novel wind energy systems produce wakes with annular cross-sections, which are qualitatively different from the wakes with circular cross-sections commonly generated by conventional horizontal-axis wind turbines and by compact obstacles. Since wind farms use arrays of hundreds of turbines, good analytical wake models are essential for efficient wind farm planning. Several models already exist for circular wakes (e.g. Morton, B. R., *J. Fluid Mech.* **10**:101–112, 1961); however, none have yet been proposed for annular wakes, making it impossible to estimate their array performance. We use the entrainment hypothesis to develop a reduced-order model for the shape and flow velocity of an annular wake from a generic toroidal obstacle. Our model consists of a set of three ordinary differential equations, which we solve numerically. In addition, by assuming that the annular wake does not drift radially, we further reduce the problem to a model comprising only two differential equations, which we solve analytically. Both of our models are in good agreement with previously published large eddy simulation results.

1 Introduction

Wind turbine power is determined primarily by the diameter of the turbine and its efficiency. This has led to the development of large HAWTs, with diameters of over 130 m [1]. While HAWTs have been very successful in land-based and shallow-offshore arrays, they have yet to meaningfully take advantage of other significant wind energy resources. Near-offshore HAWT windfarms have not yet achieved cost parity with conventional energy technologies [2], and far-offshore projects remain expensive [1]. Additionally, HAWTs cannot access wind resources in the upper atmosphere, where the wind power density is about two times greater than it is at typical HAWT hub heights because wind speed increases with altitude [3].

To take advantage of these currently untapped energy resources, new airborne wind energy (AWE) technologies are being developed that can harvest wind power from a tethered kite or aircraft [4, 5]. Several AWE designs consist of a large, tethered kite that flies transverse to the prevailing wind in a closed loop, allowing it to reach the faster-moving winds present higher in the atmosphere. The kite harvests energy either by a turbine generator on the kite that transmits electrical power to the base, or by transmitting mechanical power from the kite to the base. Many different designs have been developed with both of these power mechanisms, as well as with moving or stationary base stations and a variety of flight patterns [5, 6]. A commonly considered operating mode involves flying the kite along a circular path, thereby generating an annular wake; this is the case, for example, for the Makani energy kite [7]. As AWE development continues, the technology may eventually be viable for large-scale wind farms. Indeed, according to [8], global deployment of AWE systems could produce enough electricity to power the world at least three times over. However, for large-scale AWE farms to become a reality, an understanding of their wakes will be critical for determining array spacing and layout.

¹s_kaufman-martin@ucsb.edu

Surprisingly, while circular wakes have been studied extensively in both the literature on free shear flows [9, 10, 11] and in the literature on wind turbine wakes [12, 13, 14], there appear to be no theoretical models of annular wakes, to the best of our knowledge. The only existing study on annular turbine wakes appears to be a large eddy simulation of AWE kite aerodynamics by [15]. Other related works include a study by the same group on pumping-mode AWE devices [16], studies on the behavior of annular jets [17, 18], investigations on the wakes behind toroidal bluff bodies at low Reynolds number [19], and a study by [20] on the impact of kites on HAWT farm wakes.

In this paper, we develop two theoretical models for annular wakes by leveraging the concept of entrainment velocity, whose history includes applications to modeling plumes [21], wakes with circular cross-sections [22], gravity currents [23], and wind farms [24, 25]. In § 2, we derive two entrainment-based models for the shape and speed of an annular wake as a function of distance behind an annular obstacle. The first model must be solved numerically, whereas the second can be solved analytically. In § 3, we then compare the models to the simulation results from [15], finding good agreement. A discussion is presented in § 4, with conclusions following in § 5.

2 Entrainment-based models of annular wakes

2.1 Assumptions and Definitions for Models

For simplicity, it is assumed that the obstacle that generates the wake is perpendicular to a constant oncoming wind with a uniform velocity V_∞ . The distance between the inner and outer radii of the obstacle is denoted by S , and the overall diameter of the obstacle is D , as shown in figure 1(a). The obstacle is assumed to slow the airflow immediately downstream of it, according to the predictions of actuator disc theory. Unlike in a conventional (circular) axisymmetric wake, there will be a core region at the center of the annulus-shaped wake whose axial velocity V_i will initially be greater than the wake velocity V_w . The initial value of V_i should be close to V_∞ (although not necessarily identical) and may vary with distance x behind the turbine. It is assumed that the wake can be completely described by the wake velocity V_w , wake span S_w , and total diameter D_w , which depend only on x . Turbulent entrainment is expected to increase V_w , S_w , and D_w with increasing x . Following the entrainment hypothesis, fluid downstream of the obstacle is assumed to entrain into the wake at a radial velocity of $w_e = E(V_\infty - V_w)$ from the external flow, and at a radial velocity of $w_i = E(V_i - V_w)$ from the core region, where E denotes the entrainment coefficient. Similarly to other established wake models [26], the pressure in the wake is assumed to be constant (after the initial adjustment that takes place immediately behind the obstacle) and equal to the ambient pressure (see § 2.4).

2.2 Full Model: Flux Conservation in Annulus and Core

Following the approach of [22] (see also [25] for a modern treatment), equations for mass and momentum conservation were derived for the annular wake and the core region.

With reference to the wake sketched in figure 1(a), consider an axisymmetric control volume of infinitesimal length Δx in the axial direction, with radial dimensions corresponding to the inner and outer radial boundaries of the wake at the given distance x , as sketched in figure 1(b). In a given plane, the area of the core region is $\frac{\pi}{4}(D_w - 2S_w)^2$, implying that the area of the annular wake is $\frac{\pi}{4}[D_w^2 - (D_w - 2S_w)^2]$, which can be simplified to $\pi S_w(D_w - S_w)$. Assuming the fluid has uniform density, conservation of mass in the annular control volume implies that

$$\begin{aligned} \pi S_w(D_w - S_w)V_w + \pi D_w w_e \Delta x + \pi(D_w - 2S_w)w_i \Delta x \\ = \pi S_w(D_w - S_w)V_w + \frac{d}{dx} [\pi S_w(D_w - S_w)V_w] \Delta x. \end{aligned} \quad (1)$$

Dividing through by $\pi \Delta x$, canceling the first term on each side, and using the definition of the entrainment velocity given in § 2.1, the equation for conservation of mass in the annulus is

$$\frac{d}{dx} [S_w(D_w - S_w)V_w] = E(V_\infty - V_w)D_w + E(V_i - V_w)(D_w - 2S_w). \quad (2)$$

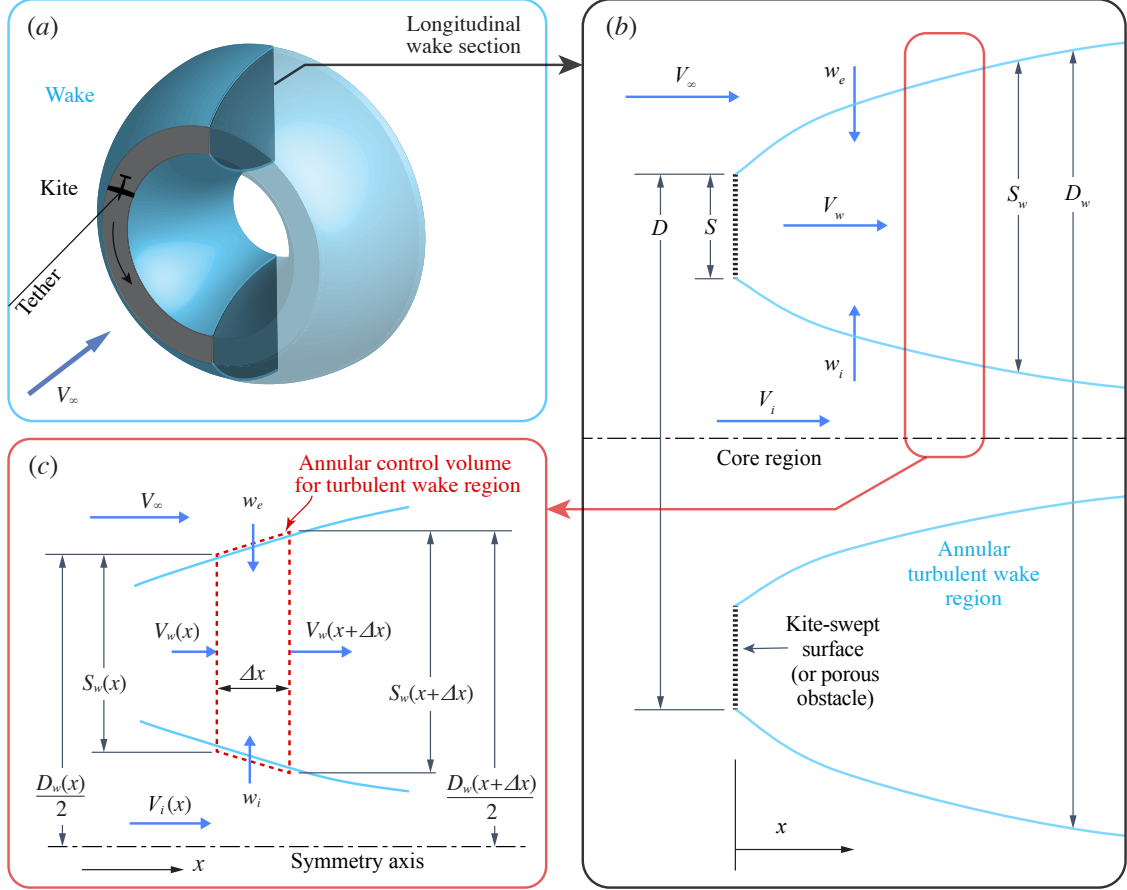


Figure 1. (a) Schematic of the development of an annular wake behind a porous obstacle or kite flying on an annular path. (b) Annular-wake cross-section, showing definitions for the entrainment model. (c) Cross-section of the annular control volume used for the turbulent wake region; for clarity, only the top portion is shown. A similar control volume analysis is used for the core region.

Assuming a negligible pressure gradient in the wake, the above approach can then be used to derive an equation for conservation of momentum in the annulus (shown below in equation 4), as well as for conservation of mass and momentum in the core region (equations 5–6). With π times the density factored out, the conservation equations are as follows, with equation (2) repeated first for clarity:

$$\frac{d}{dx} [S_w(D_w - S_w)V_w] = E(V_\infty - V_w)D_w + E(V_i - V_w)(D_w - 2S_w), \quad (3)$$

$$\frac{d}{dx} [S_w(D_w - S_w)V_w^2] = EV_\infty(V_\infty - V_w)D_w + EV_i(V_i - V_w)(D_w - 2S_w), \quad (4)$$

$$\frac{d}{dx} \left[\frac{1}{4}(D_w - 2S_w)^2 V_i \right] = -E(V_i - V_w)(D_w - 2S_w), \quad (5)$$

$$\frac{d}{dx} \left[\frac{1}{4}(D_w - 2S_w)^2 V_i^2 \right] = -EV_i(V_i - V_w)(D_w - 2S_w). \quad (6)$$

Upon closer examination, one can show that only three differential equations and one constant are necessary to fully describe the mass and momentum fluxes in this model. Using the product rule to expand the left side of equation (6) gives:

$$\frac{d}{dx} \left[\frac{1}{4}(D_w - 2S_w)^2 V_i \right] V_i + \frac{1}{4}(D_w - 2S_w)^2 V_i \frac{dV_i}{dx} = -E V_i (V_i - V_w)(D_w - 2S_w). \quad (7)$$

Multiplying equation (5) by V_i and subtracting it from equation (7) then gives:

$$\frac{1}{4}(D_w - 2S_w)^2 V_i \frac{dV_i}{dx} = 0, \quad (8)$$

which implies

$$V_i = \text{constant}. \quad (9)$$

Therefore, equations (5) and (6) are equivalent, and we retain only (3,4,5) to solve for the three remaining unknowns V_w, D_w, S_w .

In order to solve this system of differential equations numerically, a set of initial conditions (ICs) is required. Therefore, ICs are derived by applying streamtube analysis and actuator disc theory to the flow in figure 1(a). Similar to the approach of [13] for circular wakes, here we used actuator annulus theory [27] to derive the initial values of V_i, V_w, S_w , and D_w at $x = 0$. From the definition of the axial induction factor a in actuator annulus theory, it follows that $V_{w,0} = V_\infty(1 - 2a)$. The area of the annulus can then be obtained through mass conservation in the streamtube passing through the obstacle:

$$\frac{S_{w,0}(D_{w,0} - S_{w,0})}{S(D - S)} = \frac{1 - a}{1 - 2a}. \quad (10)$$

Since there is no induction in the core region, the actuator annulus model predicts that $V_{i,0} = V_\infty$. Once again, applying mass conservation in the core region provides the initial condition for the core area:

$$D_{w,0} - 2S_{w,0} = D - 2S. \quad (11)$$

Equations (10) and (11) can be combined to solve explicitly for $D_{w,0}$ and $S_{w,0}$. Thus, the ICs for the system of differential equations are as follows:

$$V_{w,0} = V_\infty(1 - 2a), \quad (12)$$

$$D_{w,0} = \sqrt{D^2 + S(D - S) \frac{4a}{1 - 2a}}, \quad (13)$$

$$S_{w,0} = S + \frac{1}{2}(D_{w,0} - D). \quad (14)$$

The fact that $V_i = \text{constant} = V_{i,0} = V_\infty$ allows us to simplify equations (3)-(5) as follows:

$$\frac{d}{dx} \left[S_w(D_w - S_w)V_w \right] = 2E(V_\infty - V_w)(D_w - S_w), \quad (15)$$

$$\frac{d}{dx} \left[S_w(D_w - S_w)V_w^2 \right] = 2E V_\infty (V_\infty - V_w)(D_w - S_w), \quad (16)$$

$$\frac{d}{dx} \left[\frac{1}{4}(D_w - 2S_w)^2 V_\infty \right] = -E(V_\infty - V_w)(D_w - 2S_w). \quad (17)$$

While the initial value problem (IVP) represented by (12)-(17) can be numerically solved as-is with software such as Wolfram Mathematica, one can simplify the equations by restating them in terms of the mass and momentum fluxes in the wake and core, such that each left-hand side in (15)-(17) is the derivative of a single dependent variable, rather than a combination of S_w, D_w , and V_w (this is a common approach for entrainment-based models in geophysics [22]). In the following definitions, m signifies mass flux and M denotes momentum flux. Once again, π times the density

has been factored out:

$$m_w \equiv S_w(D_w - S_w)V_w, \quad (18)$$

$$M_w \equiv S_w(D_w - S_w)V_w^2, \quad (19)$$

$$m_i \equiv \frac{1}{4}(D_w - 2S_w)^2V_\infty, \quad (20)$$

Using the above definitions, one can rewrite equations (15)-(17) in the following form:

$$\frac{dm_w}{dx} = 2E \left(V_\infty - \frac{M_w}{m_w} \right) \left[\sqrt{\frac{m_i}{V_\infty} + \frac{m_w^2}{M_w}} + \sqrt{\frac{m_i}{V_\infty}} \right], \quad (21)$$

$$\frac{dM_w}{dx} = V_\infty \frac{dm_w}{dx}, \quad (22)$$

$$\frac{dm_i}{dx} = -2E \left(V_\infty - \frac{M_w}{m_w} \right) \sqrt{\frac{m_i}{V_\infty}}. \quad (23)$$

The IVP represented by equations (12)-(23) was integrated using MATLAB's ode45 solver. The following definitions (rearranged versions of equations 18-20) were then used to convert the results back into the desired form:

$$V_w = \frac{M_w}{m_w}, \quad (24)$$

$$S_w = \sqrt{\frac{m_i}{V_\infty} + \frac{m_w^2}{M_w}} - \sqrt{\frac{m_i}{V_\infty}}, \quad (25)$$

$$D_w = 2\sqrt{\frac{m_i}{V_\infty} + \frac{m_w^2}{M_w}}. \quad (26)$$

Thus, results were obtained for V_w , S_w , and D_w , as a function of x (see § 3).

2.3 Analytical model: No Radial Wake Drift

While the full model produced results that were a close match to the simulations of [15] (see § 3), we were curious to see if an analytical model of the wake could be derived via a slight simplification of the control volume analysis. Therefore, a second model was derived using a different approach to the behavior of the core region, inspired by the qualitative appearance of the wake profile in the results of [15]. Instead of using the conservation equation (17) to model the core region, the center of the wake ring (located at radial distance $\frac{D_w}{2} - \frac{S_w}{2}$ from the axis of turbine rotation) is assumed to not drift from its initial position at $\frac{D_{w,0}}{2} - \frac{S_{w,0}}{2}$. Equivalently, this assumes $D_w - S_w = D_{w,0} - S_{w,0} = \text{constant}$, which is henceforth called the no radial wake drift assumption.

The governing equations for this model are mass and momentum conservation in the annulus (i.e. equations 15 and 16 from the full model) and the No Wake Drift assumption:

$$\frac{d}{dx}[S_w(D_w - S_w)V_w] = 2E(V_\infty - V_w)(D_w - S_w), \quad (27)$$

$$\frac{d}{dx}[S_w(D_w - S_w)V_w^2] = 2EV_\infty(V_\infty - V_w)(D_w - S_w), \quad (28)$$

$$D_w - S_w = D_{w,0} - S_{w,0}. \quad (29)$$

Since we assumed that $D_w - S_w$ is a constant, this term can be factored out of (27) and (28). Multiplying (27) by V_∞ and subtracting (28) gives:

$$\frac{d}{dx}[S_w V_w (V_\infty - V_w)] = 0. \quad (30)$$

Integrating, we find that:

$$S_w V_w (V_\infty - V_w) = C, \quad (31)$$

where C is a constant. A value for C can be obtained by using the same ICs (12-14) already obtained in § 2.2:

$$C = S_{w,0} V_\infty^2 2a(1 - 2a). \quad (32)$$

Solving equation (31) for S_w and substituting it into (27), one can integrate the resulting equation, solve for V_w , and find that

$$V_w = V_\infty - \sqrt{\frac{C}{4E(x - x_c)}}, \quad (33)$$

where x_c is a constant of integration. Given this result for V_w , the above equations can be combined to solve for S_w and D_w .

In summary, the No Radial Drift assumption gives a set of four equations (one constant, three variables of interest) that form a complete analytical model of an annular wake's evolution. The full set of equations is listed below:

$$x_c = -\frac{S_{w,0}(1 - 2a)}{8Ea}, \quad (34)$$

$$V_w = V_\infty \left[1 - \sqrt{\frac{S_{w,0}a(1 - 2a)}{2E(x - x_c)}} \right], \quad (35)$$

$$S_w = S_{w,0} \frac{2a(1 - 2a)V_\infty^2}{V_w(V_\infty - V_w)}, \quad (36)$$

$$D_w = D_{w,0} - S_{w,0} + S_w. \quad (37)$$

2.4 Expansion Length

As mentioned in § 2.1, the entrainment hypothesis assumes that pressure in the wake is equal to the ambient pressure. In actuality, wind turbines cause a pressure drop immediately behind the rotor. As shown during the derivation of the initial conditions in § 2.2, actuator disc theory predicts that for a short distance behind the rotor (henceforth referred to as the expansion length), the wake expands as the fluid continues to decelerate until the pressure in the wake equalizes with the ambient pressure. At this point, the regime of turbulent entrainment is expected to become dominant in the wake.

To account for the expansion length in our models, the results of both calculations are shifted forward in the x direction by an empirically-chosen constant x_e with values typically in the range of $0 < x/D < 1$. This is conceptually similar to the introduction of a virtual origin in entrainment-based plume models [28, 29].

3 Results

3.1 Numerical simulation of Ref. [15]

For the purpose of comparison with the models derived in § 2, velocity profiles from figure 5 in [15] were converted into tophat velocity profiles in the following manner. Note that U_∞ in [15] is equivalent to V_∞ in this paper. Data points with $u_x/U_\infty < 1$ are considered to be inside the wake; therefore, the surface where $u_x/U_\infty = 1$ is considered to be the wake boundary. The wake velocity V_w is considered to be the area average of u_x/U_∞ values inside the wake.

Note that the conventions for normalizing distance in [15] are different than the ones used in this paper. Ref. [15] define R as the radial distance to the midpoint of the kite, whereas in this paper, the outer radius of the kite's flight path is used. Therefore, D in this paper is equal to $2R + S$ in

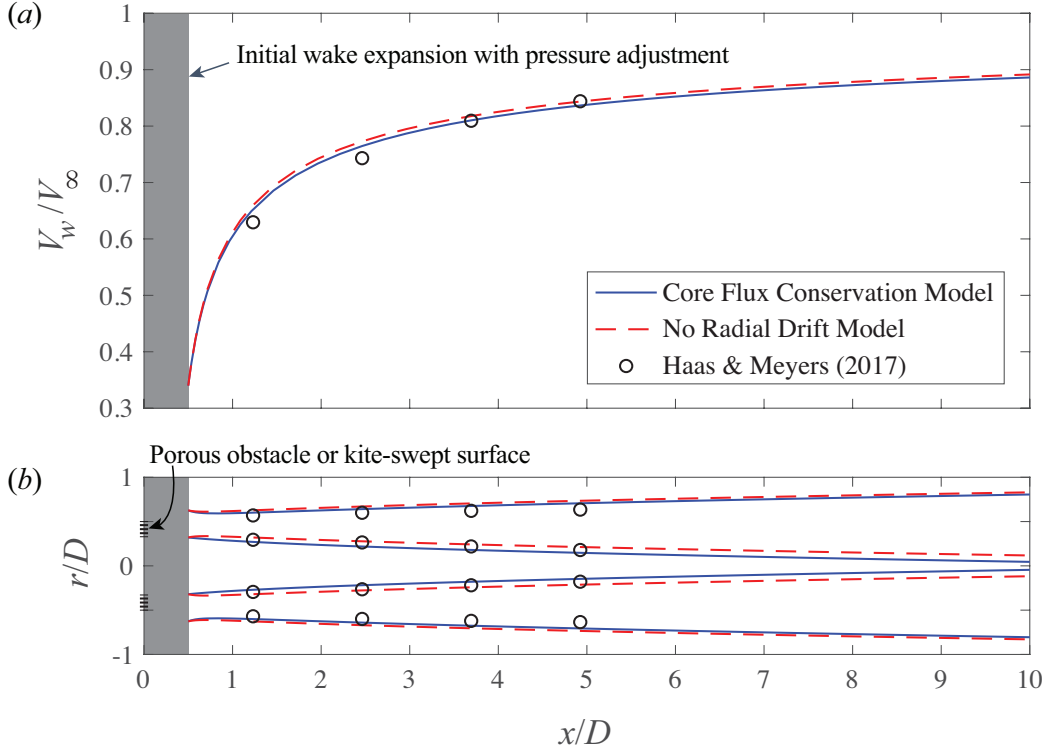


Figure 2. Laminar inflow case. (a) Wake velocity comparison between entrainment wake models and the simulation of [15]. (b) Wake boundary comparison between entrainment wake models and the simulation of [15]. Outer curves are $\pm \frac{D_w}{2}$; inner curves are $\pm(\frac{D_w}{2} - S_w)$ (equivalent to $\pm \sqrt{\frac{m_i}{V_\infty}}$).

[15]. The data of [15] used in figure 2 have been scaled to match the coordinate system defined in figure 1(a).

3.2 Parameters for models and results

The key parameters (independent variables) used as inputs for our models were made to be the same as in [15], i.e. $S/D = 0.18$ and $a = 0.33$.

Our models also use the empirical constant E , which is typically around 0.15 for HAWT models in low-turbulence inflow [25] but can reach up to 0.6 for high-turbulence plumes and jets [28], and the expansion length x_e , which is typically in the range of $0 < x/D < 1$. When choosing values of E and x_e , only the fit of the models' predictions with the velocity data from [15] was considered, as opposed to attempting to fit both the wake shape and the velocity. This is because the “wake boundary” is an artificially-defined parameter compared to the wake velocity, and the wake velocity is the most important parameter for wind farm planning. To model the laminar inflow case from [15], both models use $E = 0.15$ and $x_e = 0.5D$. For the turbulent inflow case, both models use $E = 0.5$ and $x_e = 0.5D$. A comparison between our models and [15] is shown in figure 2 (laminar) and figure 3 (turbulent).

4 Discussion

In the region of the wake for which the entrainment hypothesis is valid ($x/D \gtrsim 1$), the velocity predictions of both the Core Flux Conservation Model (full model) and the No Radial Drift Model (analytical model) show good agreement with the simulation data from [15] in both the laminar and

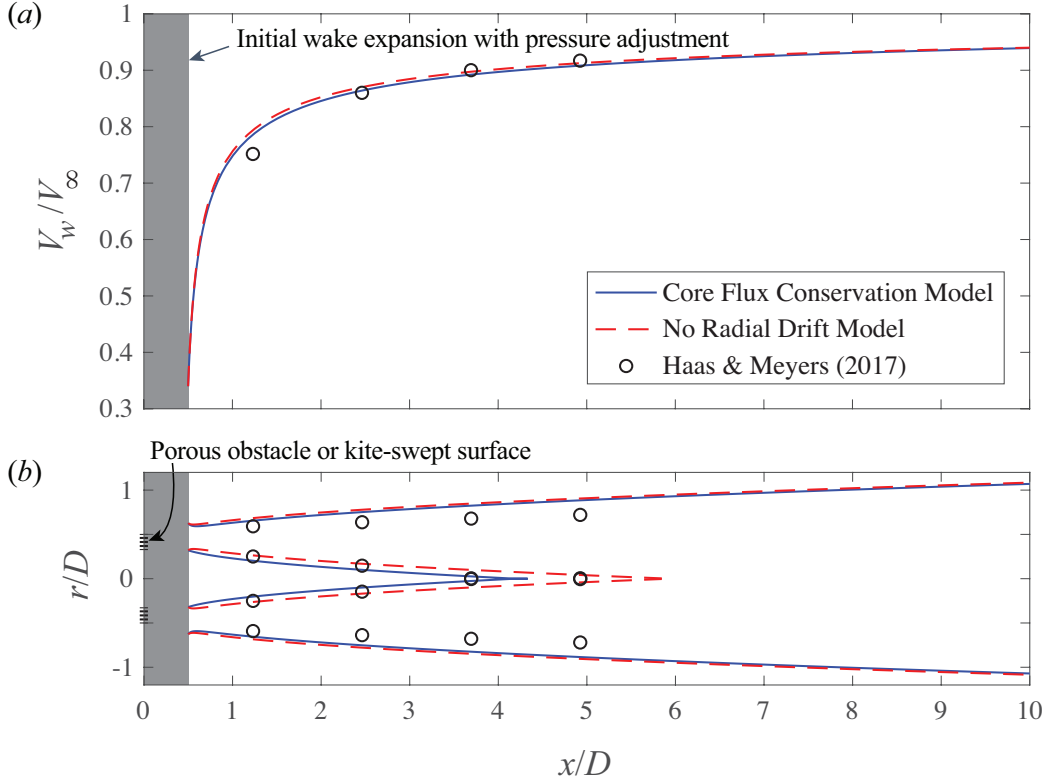


Figure 3. Turbulent Inflow Case. (a) Wake velocity comparison between entrainment wake models and the simulation of [15]. (b) Wake boundary comparison between entrainment wake models and the simulation of [15]. Outer curves are $\pm \frac{D_w}{2}$; inner curves are $\pm(\frac{D_w}{2} - S_w)$ (equivalent to $\pm\sqrt{\frac{m_i}{V_\infty}}$).

turbulent inflow cases. There appears to be little difference between the velocity results of the two models.

The main difference between the two solutions is that the full model correctly captures the wake-merging behavior in the turbulent case, whereas the analytical model does not (see figure 3). In the full model, once $\frac{D_w}{2} - S_w$ (equivalent to $\sqrt{\frac{m_i}{V_\infty}}$) reaches 0 (i.e. the wake's annulus merges and eliminates the core region), $\frac{D_w}{2} - S_w$ remains at 0 for all subsequent values of x/D . On the other hand, in the analytical model, $\frac{D_w}{2} - S_w$ continues past 0 and becomes negative, so the user of the model must know to ignore this erroneous behavior and focus only on the behavior of the outer wake boundary ($\frac{D_w}{2}$), which is still reasonably accurate. This difference between the models is unsurprising given that the Core Flux Conservation Model conserves mass in the core region, whereas the No Radial Drift Model ignores core mass conservation in favor of a geometrically simplified approach that permits an analytical solution.

When the core region is eliminated as the wake annulus merges, one can switch to the traditional, analytical wake model of [22, 25], using the values of V_w and D_w at merger as the new initial conditions. For the full annular wake model, this would save computational effort while retaining accuracy, which could be valuable in wind farm optimization applications.

The models introduced here are not restricted to airborne wind energy applications. For example, they could describe the wakes of ground-based annular wind turbines (such as the one in [30]). With different initial conditions, they could potentially also be applied to the wakes of other toroidal obstacles. The existing initial conditions would be replaced by a matching condition between the momentum deficit and the drag on the obstacle, and a development length that could be found empirically, similarly to approaches for conventional wakes [26].

5 Conclusion

By using the entrainment hypothesis and considering mass and momentum budgets behind a toroidal obstacle, we derived a model for the spatial development of a turbulent annular wake. Initial conditions were obtained from actuator annulus theory. The model consists of three coupled ordinary differential equations, which are solved numerically. By assuming negligible radial drift in the turbulent wake, we also derived a simplified model, which admits an analytical closed-form solution.

Both models appear to compare well with existing data, especially for larger x/D values. To help provide an even stronger test of the models developed here, experimental or computational results for larger x/D would be helpful, especially given that spacing in wind turbine arrays is typically between $5 \leq x/D \leq 10$.

If supported by additional data from experiments or simulations of annular wakes, the models put forth in this paper would enable the modeling of AWE kite wakes at a much lower computational cost than existing methods. This would greatly facilitate the planning of AWE wind farms, which in turn could enable society to harvest previously untapped, energy-dense wind resources.

6 Declaration of Interests

The authors report no conflict of interest.

References

1. Xiaojing Sun, Diangui Huang, and Guoqing Wu. The current state of offshore wind energy technology development. *Energy*, 41(1):298–312, 2012.
2. U.S. Energy Information Administration. Levelized cost and levelized avoided cost of new generation resources in the annual energy outlook 2019. Technical report, February 2019.
3. Philip Bechtle, Mark Schelbergen, Roland Schmehl, Udo Zillmann, and Simon Watson. Airborne wind energy resource analysis. *Renewable Energy*, 141:1103–1116, 2019.
4. Miles L Loyd. Crosswind kite power (for large-scale wind power production). *Journal of energy*, 4(3):106–111, 1980.
5. Antonello Cherubini, Andrea Papini, Rocco Vertechy, and Marco Fontana. Airborne wind energy systems: A review of the technologies. *Renewable and Sustainable Energy Reviews*, 51:1461–1476, 2015.
6. Uwe Ahrens, Moritz Diehl, and Roland Schmehl. *Airborne wind energy*. Springer Science & Business Media, 2013.
7. Doug Mcleod and Charlie Nordstrom. Lessons learned from testing Makani’s energy kite offshore. Airborne Wind Energy Conference 2019, October 2019.
8. Cristina L Archer, Luca Delle Monache, and Daran L Rife. Airborne wind energy: Optimal locations and variability. *Renewable Energy*, 64:180–186, April 2014.
9. M. S Uberoi and P. Freymuth. Turbulent energy balance and spectra of the axisymmetric wake. *Phys. Fluids*, 13(9):2205–2210, 1970.
10. I Eames, P B Johnson, V Roig, and F Risso. Effect of turbulence on the downstream velocity deficit of a rigid sphere. *Phys. Fluids*, 23(9):095103, September 2011.
11. J. Nedić, J. C. Vassilicos, and B. Ganapathisubramani. Axisymmetric turbulent wakes with new nonequilibrium similarity scalings. *Phys. Rev. Lett.*, 111(14):144503, 2013.

12. Niels Otto Jensen. A note on wind generator interaction. Technical Report RISØ-M-2411, Risø National Laboratory, 1983.
13. Sten Frandsen, Rebecca Barthelmie, Sara Pryor, Ole Rathmann, Søren Larsen, Jørgen Højstrup, and Morten Thøgersen. Analytical modelling of wind speed deficit in large offshore wind farms. Wind Energy, 9(1-2):39–53, January 2006.
14. M. Bastankhah and F. Porté-Agel. A new analytical model for wind-turbine wakes. Renewable Energy, 70(C):116–123, 2014.
15. T Haas and J Meyers. Comparison study between wind turbine and power kite wakes. J. Phys. Conf. Ser., 854(1):012019, June 2017.
16. T Haas, J De Schutter, M Diehl, and J Meyers. Wake characteristics of pumping mode airborne wind energy systems. J. Phys. Conf. Ser., 1256:012016, July 2019.
17. W T Chan and N W M Ko. Coherent structures in the outer mixing region of annular jets. J. Fluid Mech., 89(3):515–533, December 1978.
18. John M Kuhlman. Variation of entrainment in annular jets. AIAA Journal, 25(3):373–379, March 1987.
19. T Leweke and M Provansal. The flow behind rings: bluff body wakes without end effects. J. Fluid Mech., 288:265–310, April 1995.
20. Evangelos Ploumakis and Wim Bierbooms. Enhanced kinetic energy entrainment in wind farm wakes: Large eddy simulation study of a wind turbine array with kites. In Airborne Wind Energy, pages 165–185. Springer, 2018.
21. B R Morton, Geoffrey Ingram Taylor, and John Stewart Turner. Turbulent gravitational convection from maintained and instantaneous sources. Proc. R. Soc. Lond. A Math. Phys. Sci., 234(1196):1–23, 1956.
22. BR Morton. On a momentum-mass flux diagram for turbulent jets, plumes and wakes. Journal of Fluid Mechanics, 10(1):101–112, 1961.
23. T H Ellison and J S Turner. Turbulent entrainment in stratified flows. J. Fluid Mech., 6(3):423–448, October 1959.
24. Paolo Luzzatto-Fegiz and Colm-Cille P Caulfield. Entrainment model for fully-developed wind farms: Effects of atmospheric stability and an ideal limit for wind farm performance. Phys. Rev. Fluids, 3(9):093802, September 2018.
25. Paolo Luzzatto-Fegiz. A one-parameter model for turbine wakes from the entrainment hypothesis. J. Phys. Conf. Ser., 1037(7):072019, June 2018.
26. S. B. Pope. Turbulent Flows. Cambridge University Press, 2000.
27. Peter Jamieson. Innovation in wind turbine design. Wiley, Hoboken, N.J., 2011.
28. Thomas J Overcamp and Tsunchia Ku. Effect of a virtual origin correction on entrainment coefficients as determined from observations of plume rise. Atmos. Environ., 20(2):293–300, January 1986.
29. Colm-Cille P Caulfield and Andrew W Woods. Plumes with non-monotonic mixing behaviour. Geophys. Astrophys. Fluid Dyn., 79(1-4):173–199, August 1995.
30. Andrew Porteous, Bryan Kaiser, Svetlana Poroseva, Cody Bond, and Rob Hovsapiian. Wake flow simulations for a Mid-Sized rim driven wind turbine. In 32nd AIAA Applied Aerodynamics Conference, AIAA AVIATION Forum. American Institute of Aeronautics and Astronautics, June 2014.